An ab Initio Study on the Effect of Carbon Surface Curvature and Ring Structure on $N_2(O_2)$−Carbon Intermolecular Potentials

Jeffery B. Klauda,*,† Jianwen Jiang,‡ and Stanley I. Sandler‡

Laboratory of Biophysical Chemistry, NHLBI, National Institutes of Health, Building 50, Room 3308, 50 South Drive, Bethesda, Maryland 20892, and Center for Molecular and Engineering Thermodynamics, Department of Chemical Engineering, University of Delaware, Newark, Delaware 19716

Received: December 17, 2003

The effect of carbon surface curvature and ring structure on the gas−carbon interaction potential is not well understood. Potentials derived from gas−graphite adsorption measurements are commonly used in molecular simulations with curved carbon surfaces, e.g., nanotubes, fullerenes, and other nanoporous carbons. Presented here are quantum mechanical (QM) calculations of the interactions of nitrogen and oxygen with three carbon surfaces of different curvatures (graphite, C_{60} fullerene, and C_{168} schwarzite). Generally, QM calculations at the CCSD(T) level are required to obtain accurate interaction energies for these systems; here a recently developed, computationally efficient Hybrid Method for Interaction Energies (HM-IE) of comparable accuracy was used. Atom-site intermolecular potentials fit to the quantum mechanical results produce accurate predictions of the experimentally measured second virial coefficient of adsorption for nitrogen on graphite. The QM-based gas−carbon potentials for C_{60} and C_{168} were found to be different than for graphite, and result in increased adsorption energies for nitrogen on these surfaces. We conclude that molecular simulations based on the assumption that the gas−carbon interaction potentials are invariant to carbon surface curvature and ring structure may result in incorrect property predictions.

Introduction

The industrial separation of nitrogen and oxygen from air is usually accomplished by using energy-intensive cryogenic distillation. However, membranes offer the possibility of a more energy-efficient separation technique. Polymeric membranes can be used to separate gases,[1] but only at ambient conditions. Ceramic membranes, such as zeolites, sol−gels, and nanoporous carbons (NPCs), can be used to separate gases at the harsh operating conditions that commonly occur in reactive separations.

Nanoporous carbon membranes are of interest here because of the recent discovery by Shiflett and Foley[2,3] that certain NPC membranes result in permeability ratios of O_2 to N_2 as high as 30 to 1. The synthesis of these NPC membranes consisted of the ultrasonic deposition of poly(furfuryl alcohol) (PFA) in solution on porous stainless steel. Then pyrolysis was used to form a membrane layer of solid carbon on the stainless steel support. It has been found that the O_2/N_2 permeability ratio depends on how the membrane is made, e.g., amount of material deposited, additives to PFA solution, and pyrolysis temperatures.[2] However, it is unclear what properties of the NPC membrane cause variations in the O_2/N_2 permeability ratios of from 30:1 to 2:1. The NPC membranes synthesized by Shiflett and Foley[2,3] are amorphous, but nanostructured with a narrow distribution of pore sizes. Although the exact structure is unknown, the carbon hybridization is believed to be sp^2 with hydrogen/carbon ratios that range from 0.0001 to 0.5.

Molecular dynamics and Monte Carlo simulations are excellent tools to improve our understanding of diffusion and adsorption of nitrogen and oxygen in carbon structures. Essential to these simulations are accurate gas−carbon interaction potentials. Typically, the gas−carbon intermolecular potentials used in molecular simulations have been obtained from either fits to gas adsorption on exfoliated graphite sheets[4,5] or by the use of the Lorentz−Berthelot combining rules with estimated 6-12 Lennard-Jones (LJ) parameters.[6−8] However, these potentials ignore the difference in electronic structure between flat graphite sheets and the curved surfaces in the NPC membranes. The nature of sp^2 orbitals may differ between graphite and the NPCs because graphite sheets consist of only six-membered rings, while NPCs have five-, six-, seven-, and eight-membered rings; in addition, the curved carbon surface may also result in distortion of the sp^2 orbitals. Recently Kostov et al.[9] argued that in nanotubes with high curvature, and therefore small radii, the carbon hybridization approaches sp^3 resulting in more attractive gas−carbon interactions. Therefore, graphite-based potentials[4,5] may not be applicable for carbons with a different ring structure and/or curvature.

Here ab initio quantum mechanics (QM) is used to better understand the effect of carbon surface curvature and ring structure on nitrogen−carbon and oxygen−carbon interactions. Previously, Klauda and Sandler[10] developed a method to obtain gas−water intermolecular potentials from QM for use in gas hydrate predictions. In their method, the hydrate cage of water molecules was cut into segments so that gas−cage interaction could be calculated with large basis sets and including non-pairwise-additive multibody effects by considering the contributions from a number of cage segments. The success in predicting gas adsorption in hydrate cavities[10] suggests that this method can also be used for gases adsorbing on nanoporous carbon membranes.

Since the NPC structure of Shiflett and Foley[2,3] is amorphous and unknown, a C_{60} fullerene (buckyball) and a carbon

* Author to whom correspondence should be addressed. E-mail: klauda@helix.nih.gov. Phone: (301) 496-9510. Fax: (301) 402−3404.
† National Institutes of Health.
‡ University of Delaware.

10.1021/jp037897h CCC: $27.50
Published on Web 06/15/2004

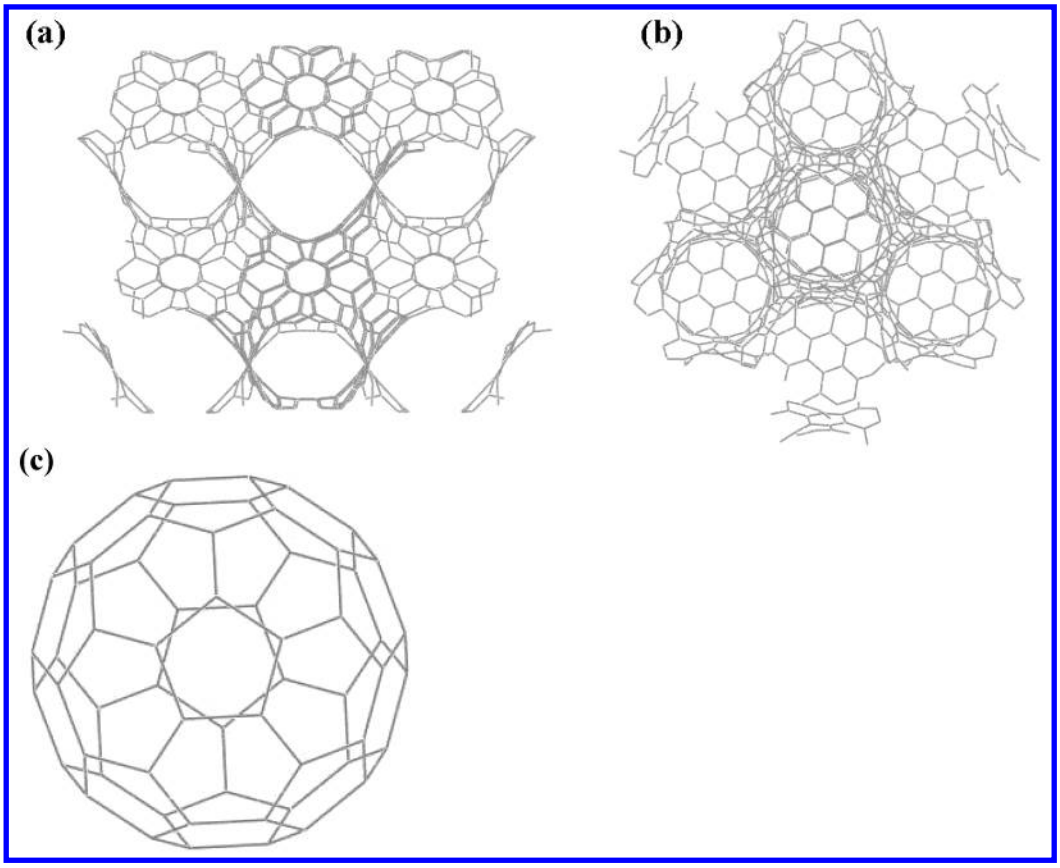

Figure 1. A singe cubic unit cell of C_{168} with projections as seen from (a) the (110) direction, (b) the (111) direction, and (c) a C_{60} fullerene.

schwarzite are used here as models for an NPC to assess the likely effects of surface curvature. The carbon schwarzite structure is similar to an amorphous NPC, but consists of a repeating unit cell with a defined structure. These structures are named for the mathematician who first explored these triply periodic minimal surfaces with negative curvature.[11] A large number of unique carbon structures can be formed from the three types of periodic surfaces (D, P, and G),[12] each having different pore sizes and electrical properties.[13] These structures can be energetically more stable than the C_{60} fullerene, though they have not yet been made.[14−17] For this study, the C_{168} structure proposed by Vanderbilt and Tersoff[15] consisting of six- and seven-membered rings was investigated. Two projections of the C_{168} cubic unit cell are shown in Figure 1, where two distinct convex lens channels are protruding toward the viewer in Figure 1a. In the center of Figure 1b is a channel intersection resulting from four tetrahedral channels. In addition, gas interactions with the C_{60} buckyball[18,19] (Figure 1c) are also studied to elucidate the effect of the five-membered carbon rings that are not present in carbon schwartzites, as the carbon surface curvatures in the C_{60} fullerene and C_{168} schwarzite are nearly identical.[15]

Here the interactions of the gases with benzene and graphite are first studied to choose the QM methods to be used in the development of the interaction potentials for N_2 and separately O_2 with the curved carbon surfaces. Since benzene is smaller than the carbon clusters used in modeling carbon surfaces, it serves as a useful test case to survey different QM methods and determine which is appropriate for these systems. Having developed an acceptable method, the N_2−graphite interaction energies so obtained are then fit to an analytic potential and used for comparison with a published empirical potential that had been obtained by fitting adsorption measurements. Next, QM interaction energies are calculated for O_2 and N_2 with the curved carbon surfaces of the C_{60} buckyball and C_{168} schwarzite, and analytic interaction potentials are developed. In the final section, the flat surface, curved surface, and empirical gas−carbon potentials are compared.

Methods

Interactions between nitrogen and benzene were studied first to determine the appropriate QM method (MP2, MP3, MP4, or CCSD(T)) to be used for surface segments containing large numbers of carbon atoms. Nitrogen−benzene interactions have been studied previously with DFT[20] and MP2,[21] but the results were inaccurate. Lee et al.[22] found that CCSD(T) calculations were required to accurately predict the experimental rovibrational spectra for this system. Also Klauda et al.[23] found that CCSD(T) or methods that approximate CCSD(T) energies with a large basis set are required to obtain accurate nitrogen−benzene interactions. We will demonstrate in the following paragraphs that CCSD(T) is required to obtain accurate nitrogen−benzene interactions and for other carbon surfaces studied here.

In our calculations, the geometry of the benzene molecule[24] was fixed with $R_{CC} = 1.40$ Å, $R_{CH} = 1.10$ Å, and $\angle CCC = 120°$; and the bond length of nitrogen was fixed at 1.10 Å. The 6-31+G(3d) basis set, which accurately reproduces the polarizability and quadrupole moment of N_2 at the MP2 level, was used to determine the appropriate approximation to the Hamiltonian and the wave function. For nitrogen with its center of mass located 3.2 Å over the center of, and parallel to, the benzene ring, and nitrogen's projected axis bisecting two carbon−carbon bonds, the counterpoise-corrected HF, MP2, MP3, MP4(SDQ), and CCSD(T) interaction energies were found to be +9.5, −7.4, −1.2, −1.5, and −3.4 kJ/mol, respectively. Note that the more accurate CCSD(T)/6-31+G(3d) binding

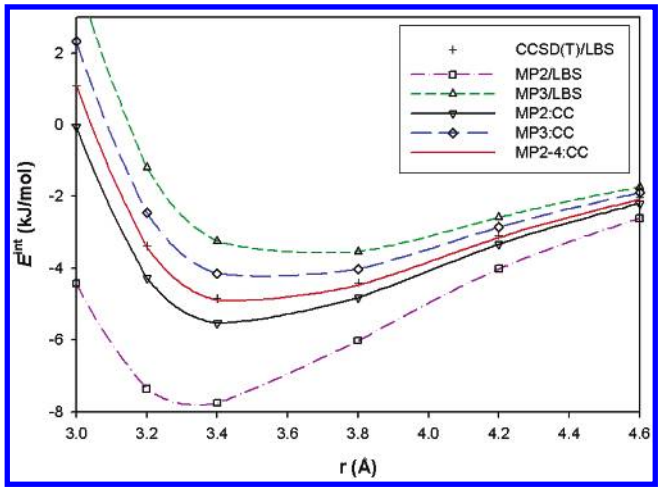

Figure 2. Interaction energies between N_2 and C_6H_6 with the N_2 axis parallel with the C_6H_6 plane: SBS is 3-21G*, MBS is 6-31G(d), and LBS is 6-31+G(3d).

energy is less than 50% of that from the MP2/6-31+G(3d) calculation. Similar variations are observed for the Møller−Plesset and CCSD(T) interaction energies with triple-ζ basis sets of 6-311+G(d) and 6-311+G(3d), i.e., a 73% and 52% reduction in the binding energy with CCSD(T) rather than MP2. These calculations and previous work[22,23] demonstrate that the computationally intensive CCSD(T) method is required for accurate $N_2-C_6H_6$ interaction energies. However, current processor speed and available disk space prohibit the use of CCSD(T) with a sufficiently large basis set for the gas−graphite, gas−fullerene, or gas−carbon schwarzite systems when using a large number of carbon atoms to represent the surface and its curvature.

A previously developed QM hybrid method referred to as HM-IE[23] (the **H**ybrid **M**ethod for **I**nteraction **E**nergies), provides accurate estimates of the interaction energy calculated by CCSD(T) with a large basis set, but requires considerably less computational time and resources.[23] Similar to the Gaussian-3 (G3) methods of Curtiss et al.,[25,26] or related approaches of Dunning and Peterson,[27] and others,[28−33] HM-IE assumes that the effects of electron correlation and basis set size are additive. In the G3 methods, high-level energy calculations, e.g., QCISD(T), are performed with small basis sets, and lower level calculations (MP2 and MP4) are performed with larger basis sets. These are then combined in the G3 method to yield accurate heats of formation, ionization potentials, electron affinities, and proton affinities in calculations that are much faster than QCISD(T) with large basis sets.[25,26] Dunning and Peterson[27] approximated the basis set dependence of CCSD(T) results with that of the Møller−Plesset perturbation methods for various properties.

The details of HM-IE can be found elsewhere;[23] the calculation of interaction energies, E^{int}, is as follows,

$$\begin{aligned} E^{int}[\text{CCSD(T)/LBS}] &= E^{int}[\text{CCSD(T)/SBS}] + (E^{int}[\text{CCSD(T)/LBS}] - E^{int}[\text{CCSD(T)/SBS}]) \\ &\cong E^{int}[\text{CCSD(T)/SBS}] + (E^{int}[\text{MPn/LBS}] - E^{int}[\text{MPn/SBS}]) \\ &\equiv E^{int}[\text{MPn:CC}] \end{aligned} \quad (1)$$

where SBS denotes the small basis set, LBS denotes the large basis set, and MPn with $n = 2$, 3, or 4 is generic for MP2, MP3, and MP4(SDQ). For MPn:CC (also referred to as single-step HM-IE), the basis set contribution going from the CCSD(T)/SBS to the CCSD(T)/LBS levels is approximated by the difference between the interaction energies at the MPn levels with the same basis sets. A combination hybrid method, MP2/3:CC,

$$E^{int}[\text{MP2/3:CC}] = {}^1/_2(E^{int}[\text{MP2:CC}] + E^{int}[\text{MP3:CC}]) \quad (2)$$

was found previously to accurately represent interaction energies of Ne_2, $(C_2H_2)_2$, and N_2-benzene.[23] However, for the larger surfaces of C_{60} and C_{168} of interest here, the MP2/3:CC method in eq 2 required more disk space than the 16GB limit of Gaussian 98[34] on 32-bit processors. A further reduction in computational requirements can be achieved with the following two-step HM-IE approach (MP2−4:CC),

$$\begin{aligned} E^{int}[\text{CCSD(T)/LBS}] &\cong E^{int}[\text{CCSD(T)/SBS}] + (E^{int}[\text{MP4(SDQ)/MBS}] - E^{int}[\text{MP4(SDQ)/SBS}]) + (E^{int}[\text{MP2/LBS}] - E^{int}[\text{MP2/MBS}]) \\ &\equiv E^{int}[\text{MP2} - \text{4:CC}] \end{aligned} \quad (3)$$

which is similar to the multiple-step approaches used in G3.[25,26] Here MBS refers to a medium-sized basis set. We reduced or removed the basis set superposition error (BSSE) in all interaction energy calculations by using the counterpoise correction method of Boys and Bernardi.[35]

Equation 3 is used in this work to approximate the CCSD(T)/LBS results. Three sets of calculations are required: (1) the CCSD(T)/SBS calculation, which includes the MP4/SBS calculations; (2) the MP4/MBS calculation, which includes the MP2/MBS calculation; and (3) the MP2/LBS calculation. Although HM-IE involves a larger number of QM calculations, it requires significantly less computational time than CCSD(T)/LBS, as will be shown shortly, since smaller basis sets are used.

Three nitrogen orientations at various separation distances were used to test the two-step HM-IE (eq 3), all with a 90° angle between the COM of nitrogen, the center of the benzene ring, and every carbon atom: (1) N_2 axis parallel to the C_6H_6 plane and projected axis bisecting two carbon−carbon bonds; (2) N_2 axis perpendicular to the C_6H_6 plane; and (3) N_2 axis at 45° to the normal of the C_6H_6 plane.

Shown in Figure 2 are the results of our QM calculations for nitrogen parallel to the benzene plane. The 6-31+G(3d) basis set was chosen as the LBS, because CCSD(T) calculations with the 6-311+G(3d) basis set only result in a small 0.08 kcal/mol (0.3 kJ/mol) increase in the binding energies compared to the double-ζ basis set of 6-31+G(3d) for the case of N_2 being parallel to the benzene plane and a separation distance of 3.2 Å between the COMs. This quite small increase in the interaction energy with a higher angular momentum basis set may be the result of this 14-atom calculation containing basis sets distributed throughout space, which is different from calculating interactions involving only small molecules that require very large basis sets due to their limited number of atoms and therefore the total number of basis functions. In addition, current computational resources prohibit calculations with a sufficiently sized triple-ζ basis set for the larger carbon clusters discussed in the following section. For the single-step HM-IE, eq 1, the 6-31G(d) basis set was used for the SBS and for the two-step HM-IE, eq 3, the 6-31G(d) and 3-21G* basis sets were used for the MBS and SBS, respectively.

The CCSD(T)/LBS global minimum in our calculations is −4.8 kJ/mol at a N_2 COM distance of 3.4 Å from the benzene plane with the N_2 axis parallel to the benzene plane. As shown previously, both MP2/LBS and MP3/LBS poorly represent the CCSD(T)/LBS interaction energies (Figure 2).[23] The MP2:CC and MP3:CC calculations still deviate from the CCSD(T)/LBS results, but to a lesser extent. However, the MP2−4:CC energies are nearly identical with the CCSD(T)/LBS results with an average absolute deviation (AAD) of only 0.046 kJ/mol for all the points shown in Figure 2. The results of the MP2/3:CC method are not shown in Figure 2; they are similar to the MP2−4:CC predictions with an AAD of 0.015 kJ/mol for the points in Figure 2.[23]

Similar results were obtained for the other nitrogen orientations. Overall, the MP2/3:CC and MP2−4:CC methods led to the best approximation of the CCSD(T)/LBS results. For a total of 17 N_2−C_6H_6 orientations, AADs of 0.82, 0.92, 0.09, and 0.19 kJ/mol from the computationally intensive CCSD(T)/LBS results were found for the MP2:CC, MP3:CC, MP2/3:CC, and MP2−4:CC methods, respectively. In addition to good accuracy compared with the CCSD(T)/LBS results, the hybrid methods significantly reduce the computational cost. For CCSD(T)/LBS calculations, one N_2−benzene orientation requires about 100 h of CPU time on an AMD MP 1800+ processor while the MP2:CC, MP3:CC, MP2/3:CC, and MP2−4:CC calculations require only 3, 7, 7, and 4 h of CPU time, respectively. [All CPU times reported in this paper are for the AMD MP 1800+ processor.]

For the oxygen−benzene calculation, the SBS, MBS, and LBS were the same as for N_2−benzene interactions, but since oxygen is an open shell molecule the spin unrestricted determinant was used with spin projection. Similar advantages in computational accuracy and load were found by using the HM-IE methods for the few O_2 orientations studied, and again the hybrid MP2/3:CC and MP2−4:CC methods were superior to the others.

The MP2/3:CC method is slightly more accurate than the MP2−4:CC method, but is too computationally demanding for larger carbon clusters. Therefore, the MP2−4:CC method was used for the interactions of oxygen and nitrogen with graphite, C_{60} fullerene, and C_{168} schwarzite.

Ab Initio Interaction Energies and Potential Fits

Graphite. The interaction between nitrogen and graphite was investigated so that a comparison to a potential fitted to adsorption measurements could be made. To cut the graphite sheet into pieces small enough for the calculation of accurate interaction energies, covalent bonds need to be broken. In our models, these bonds were terminated with hydrogen atoms placed along the cleaved bonds at a distance of 1.07 Å from the carbon atom.

Feller and Jordan[36] investigated the dependence of the water−carbon binding energy on the number of carbon atoms used to model a graphite sheet. It was found that the total water−graphite interaction energy (corrected for BSSE) changed by less than 10% from 24 to 96 carbon atoms.[36] Therefore, we used 30 carbons in a plane (see Figure 3a) to model a graphite sheet, with hydrogens added to terminate dangling bonds. Even this model is too big for calculating the interaction energies required for HM-IE in a reasonable amount of CPU time. Shown by the red and blue lines in Figure 3a are Cuts 1 and 2, respectively, in which Cut 1 contains 15 carbons in each segment (15−15) and Cut 2 has 14−16 carbons per segment. For each segment, a hydrogen atom is added along each cleaved carbon bond to maintain a similar electronic structure to that of the 30-carbon piece.

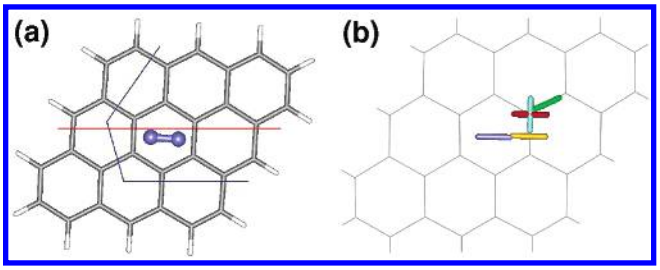

Figure 3. $C_{30}H_{14}$ used to model a graphite sheet: (a) Cut 1 along the red line and Cut 2 along the blue; (b) calculated nitrogen orientations—center in dark blue, off-center 1 in red, off-center 2 in yellow, off-center 3 in green, and off-center 4 in light blue.

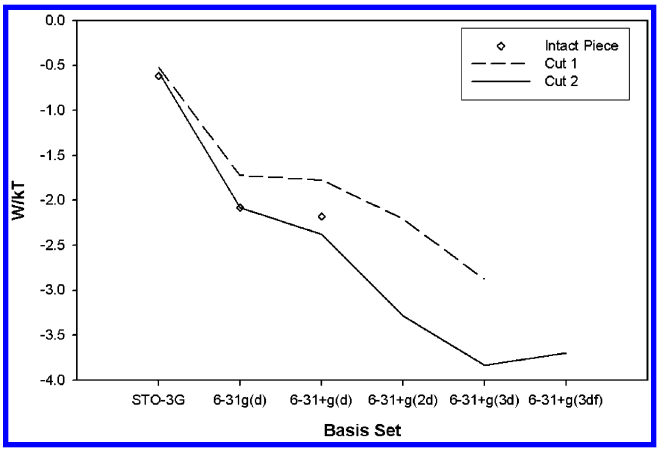

Figure 4. N_2−C_{30} MP2 interaction energies as a function of basis set scaled to 298 K at the Steele potential minimum.

The two-step HM-IE (eq 3) method was used to develop a nitrogen−graphite potential. The total interaction energy between C_{30} and nitrogen is approximated as the sum of the interactions of nitrogen and the two segments, e.g., for Cut 2 the interaction energies of nitrogen and the 14- and 16-carbon segments was summed to obtain the total N_2−C_{30} interaction energy. This sum was compared to the interaction energies with the intact C_{30} section by using several basis sets to determine the cut that best represents the nitrogen−C_{30} interaction; a similar procedure was used in our previous work on gas hydrates.[10]

While CCSD(T) is required for accurate interaction energies with graphite, it is too computationally intensive to use to determine the appropriate cuts to C_{30}. However, the results of the HM-IE method[23] demonstrated that the effect of an increase in basis set on the interaction energy is almost independent of the level of electron correlation (MP2, MP3, or CCSD(T)). As a result, for a given gas molecule orientation, the gas−carbon MP2 interaction energy as a function of basis set is shifted with respect to the CCSD(T) results, but only by a constant. Therefore, the computationally efficient MP2 was used to determine the appropriate cut of the carbon surface and the appropriately sized large basis set to be used in the HM-IE calculations. Then, the MP2−4:CC hybrid method was used to approximate the CCSD(T)/LBS interaction energies.

As seen from the results in Figure 4, Cut 2 is better than Cut 1 in representing the interaction energy for the entire 30-carbon piece. In Cut 1 the image of nitrogen on the graphite plane lies on top of the axis used to cleave C_{30}, so that the closest nitrogen−carbon sheet interactions are between nitrogen and the hydrogen added to each piece, which probably results in incorrect binding energies at close separation distances. There-

TABLE 1: Nitrogen Orientations Studied for the Interactions with Graphite[a]

position	COM distance [Å]	∠NC$_{om}$P, deg	energies, kJ/mol QM	Steele	6-12 LJ	exp-6	HB
center	3.2	0	−9.742	−7.056	−9.913	−9.863	−10.146
	5.0	0	−3.334	−2.165	−2.542	−2.847	−2.237
	3.9	10	−7.314	−5.456	−6.566	−7.433	−6.016
	3.2	45	0.354	−1.316	−4.725	−3.766	−4.294
	4.2	90	−4.509	−4.809	−5.845	−6.526	−4.834
off-center 1	3.6	0	−9.259	−6.912	−8.644	−9.489	−8.176
	3.2	45	−1.742	3.040	−0.592	−0.374	−0.818
	3.6	90	−5.830	−3.620	−5.936	−5.793	−4.333
off-center 2	3.0	0	−4.742	−2.530	−6.432	−4.970	−7.636
	3.6	45	−12.930	−5.872	−7.834	−8.183	−6.907
	3.2	90	10.195	15.101	10.820	9.283	11.347
off-center 3	3.6	0	−8.525	−6.769	−8.530	−9.308	−8.146
	3.2	45	0.228	4.524	0.788	1.053	0.364
	3.6	90	−4.710	−3.147	−5.518	−5.240	−3.981
off-center 4	3.6	0	−8.867	−6.903	−8.632	−9.474	−8.082
	3.2	45	−2.827	2.552	−1.050	−0.644	−1.231

[a] The COM distance is between the COM of nitrogen and the graphite Plane and ∠NC$_{om}$P is the angle formed by a nitrogen atom, the COM of nitrogen, and a point, P, on the graphite plane shifted to go through nitrogen's COM. Also shown are the calculated, predicted, and fitted energies for these nitrogen orientations.

fore, Cut 2 was used to avoid this problem. Binding energies calculated with Cut 2 and the 6-31+G(3d) basis set were found to be a satisfactory compromise between accuracy and CPU time, as a calculation at a larger basis set, 6-31+G(3df), resulted in only a 3% decrease in the binding energy (Figure 4). In addition, on the basis of the results for N_2 interacting with benzene, the use of a triple-ζ basis set would only slightly increase the interaction energy obtained compared to CCSD-(T)/6-31+G(3d) calculations.

Interaction energies at several orientations, positions, and distances from the C_{30} piece are required to fit an intermolecular potential. Rather than choosing random nitrogen orientations and positions, the center of mass (COM) for nitrogen was placed at positions above the COM of the benzene ring (red in Figure 3b), above the center of the C−C bond (off-center 2 and 3 in Figure 3b), and above a carbon atom (off-center 1 and 4 in Figure 3b) with nitrogen orientations perpendicular, parallel, and at a 45° angle to the graphite surface normal. On the basis of the nitrogen−benzene study, the two-step HM-IE, eq 3 was used to calculate N_2−graphite interactions. The SBS, MBS, and LBS were identical with those used in the N_2−benzene calculation. The CCSD(T) convergence criteria for the energy and wave function (10^{-6} and 10^{-8} hartree, respectively) were relaxed by 1 order of magnitude from the defaults in the Gaussian package, which reduces the CPU time by about 1 day without a loss of accuracy. Even with this change, an HM-IE calculation for a single nitrogen configuration, MP2−4:CC, requires approximately 11.5 CPU days.

A total of 16 QM interaction energies were calculated with MP2−4:CC, which required over 6 months of single-processor CPU time. Five nitrogen COM positions with respect to the center of the six-membered ring, represented by the dark blue line in Figure 3b and the orientations shown in Table 1, were considered, and interaction energies were computed at varying COM distances. For the off-center 1−3 positions (see Figure 3b and Table 1) three energies were calculated for each location with nitrogen parallel to the surface and at angles of 45° and 90°. The separation distances between the COM of nitrogen and the six-membered ring near the potential minimum were used and resulted in one repulsive interaction. Only two orientations were studied for the off-center 4 case as the 90° orientation is equivalent to the off-center 2 orientation (see Figure 3b).

Three potential functions were then fit to these 16 QM-calculated energies. Previously Bojan and Steele[4,5] fit the Lennard-Jones (6-12) parameter ϵ in

$$w^{LJ}(r_{ij}) = \sum_{i=1}^{\text{no. of guest sites}} \sum_{j=1}^{\text{no. of C sites}} 4\epsilon_{ij}\left[\left(\frac{\sigma_{ij}}{r_{ij}}\right)^{12} - \left(\frac{\sigma_{ij}}{r_{ij}}\right)^{6}\right] \quad (4)$$

to measured adsorption second virial coefficients of nitrogen and oxygen on exfoliated graphite sheets using the equation

$$B_2 = \int_V \left\{\exp\left[-\frac{w_{gc}(\underline{r},\underline{\Omega})}{kT}\right] - 1\right\} \mathrm{d}\underline{r}\, \mathrm{d}\underline{\Omega} \quad (5)$$

and integrating the gas−carbon potential over a two-dimensional graphite unit cell with a substrate of seven parallel infinite graphite sheets, each separated from the others by 3.4 Å.[4,5] In their work, the collision diameter, σ, was obtained as the mean from previously reported values of a carbon atom and oxygen or nitrogen.[4,5] We refer to the potentials so obtained as the Steele potentials.

Inelastic neutron scattering has shown that the atom site LJ 6-12 potential fails to reproduce the experimentally observed anisotropic or corrugated nitrogen−graphite potential.[37,38] However, as the magnitude of the anisotropy is small, at sufficiently high temperatures nitrogen can sample all regions of this corrugated potential, so that on average the potential developed by Bojan and Steele[4,5] may be satisfactory even though it does not reproduce the local spatial variations of the underlying potential.

Three potentials were considered here to fit the QM interaction energies: the widely used atom-site LJ 6-12 potential, the exponential-6 (exp-6) potential,

$$w^{\exp-6}(r_{ij}) = \sum_{i=1}^{\text{no. of guest sites}} \sum_{j=1}^{\text{no. of C sites}} \frac{\epsilon_{ij}}{1-(6/\alpha_{ij})} \times \left[\frac{6}{\alpha_{ij}}\exp\left[\alpha_{ij}\left(1-\frac{r_{ij}}{r_{\min}}\right)\right] - \left(\frac{r_{\min}}{r_{ij}}\right)^{6}\right] \quad (6)$$

and the anisotropic 6-12 potential of Carlos and Cole[39] used by Hansen and Bruch (HB)[37] to describe the N_2−graphite interaction

$$w^{HB}(r_{ij}) = \sum_{i=1}^{\text{no. of guest sites}} \sum_{j=1}^{\text{no. of C sites}} 4\epsilon_{ij}\left[\left(\frac{\sigma_{ij}}{r_{ij}}\right)^{12}\left(1+\gamma_R\left(1-\frac{6}{5}\cos^2\theta\right)\right)-\left(\frac{\sigma_{ij}}{r_{ij}}\right)^{6}\left(1+\gamma_A\left(1-\frac{3}{2}\cos^2\theta\right)\right)\right]+e_{cq} \quad (7)$$

where γ_A and γ_R are the coefficients that modify the van der Waals attraction and overlap repulsion, respectively, θ is the angle between the graphite surface normal and the vector along the N_2 axis, and e_{cq} is the interaction between a charge on nitrogen and the local quadrupole of the carbon atom in graphite given by

$$e_{cq} = \frac{1}{2} q_i \Theta_{zz}\left[\frac{3R_{iz}^{\ 2}}{(r_{ij})^5}-\frac{1}{(r_{ij})^3}\right] \quad (8)$$

where q_i is the charge on site i, Θ_{zz} is the quadupole of the carbon atom, and R_{iz} is the distance above the graphite sheet. The attractive and repulsive anisotropic terms in eq 7 are a result of the dielectric properties of graphite, and of the charge densities of graphite and the adsorbate, respectively. For the He−graphite interaction Carlos and Cole[39] used a γ_A value of 0.4 obtained from the measured polarizability of graphite, which was assumed to be independent of adsorbate and was used by Hansen and Bruch[37] for nitrogen on graphite. Carlos and Cole[39] found that $\gamma_R = -0.54$ best fit the scattering measurements for He on graphite. For N_2 on graphite Hansen and Bruch[37] used this value for γ_R, but we found that this leads to binding energies that are too large at short nitrogen−graphite distances compared to our QM calculations. Therefore, in eq 7 we adjusted the values of ϵ_{ij}, σ_{ij}, γ_A, and γ_R to best fit the ab initio interaction energies.

The potential parameters for our fits to the QM energies and those of the Steele potential are given in Table 2. The value of the LJ ϵ/k fit to QM is 37% larger than that in the Steele potential. The inability of simple atom site potentials to capture the known anisotropy of the nitrogen−graphite potential may be the cause of this discrepancy.[37,38] In general, the Steele potential underpredicts the attraction between nitrogen and graphite compared to the results of our calculations using two-step HM-IE, as shown in Table 1. The LJ 6-12, exp-6, and HB potentials fit to the QM interaction energies all have similar deviations from the two-step HM-IE calculated energies (Table 2); the deviation of the Steele potential, which has not been fit to the calculated energies, is slightly larger.

To compare with experimental data, these potentials were used in eq 5 to predict the values of B_2. As seen in Figure 5, the empirical Steele potential and the HB potential fit to the QM energies result in second virial coefficients of adsorption that are close to the measured values, though the Steele potential slightly underpredicts, and the HB potential slightly overpredicts, the values of B_2. In contrast, the atom site LJ and exp-6 potentials result in second virial coefficients for adsorption that significantly deviate from the measured values, even though they fit the QM energies slightly better than the HB potential. Apparently, the anisotropy of the HB potential is needed to predict accurate values of B_2. It is interesting to note that the completely predicted adsorption second virial coefficients from the HB potential fitted to the quantum mechanical energies are approximately in as good agreement with the experimental data as those obtained by using the Steele potential that had been fit to the experimental data.

C_{60} Fullerene. Having demonstrated the ability of the two-step HM-IE method to predict nitrogen−graphite interactions, the interactions of nitrogen and oxygen separately with the curved carbon surface of the C_{60} fullerene were studied. The two carbon bond lengths of 1.39 and 1.45 Å and the coordinates of the carbons in C_{60} were obtained from ref 18 (see Figure 1c). The C_{60} fullerene contains five- and six-membered rings and has a curvature similar to the C_{168} schwarzite that will be discussed in the following section, but does not have seven-membered rings present in the C_{168} schwarzite and amorphous NPCs.

Similar to the graphite calculation, a 30-carbon piece (Figure 6) was used to calculate the nitrogen and oxygen interactions with carbon in C_{60}. The 30-carbon piece with hydrogens added along the cleaved carbon bonds was then cut into two segments using an identical approach to that discussed above for the interaction between the gas molecule and the 30-carbon piece. For this system the accuracy of the gas−carbon interaction depends strongly on the cut used. The 14-16 carbon cut shown in Figure 6a was found to accurately represent nitrogen interacting with the 30-carbon piece, and was used for the nitrogen−carbon interactions of the C_{60} buckyball.

TABLE 2: Carbon−Nitrogen Atom Site Potential Parameters for the Steele Potential and Those Obtained Here from the Fit to Two-Step HM-IE Calculations[a]

potential	AAD [kJ/mol]	ϵ/k [K]	σ [Å]	γ_R	γ_A	r_{min}	α
Steele[4,5]	2.89	33.4	3.36	–	–	–	–
6-12 LJ	1.30	45.829	3.270	–	–	–	–
exp-6	1.21	42.464	–	–	–	3.777	13.431
HB	1.56	37.088	3.289	−0.056	0.102	–	–

[a] The column AAD refers to average deviations of the energies computed with these potentials from those calculated from two-step HM-IE.

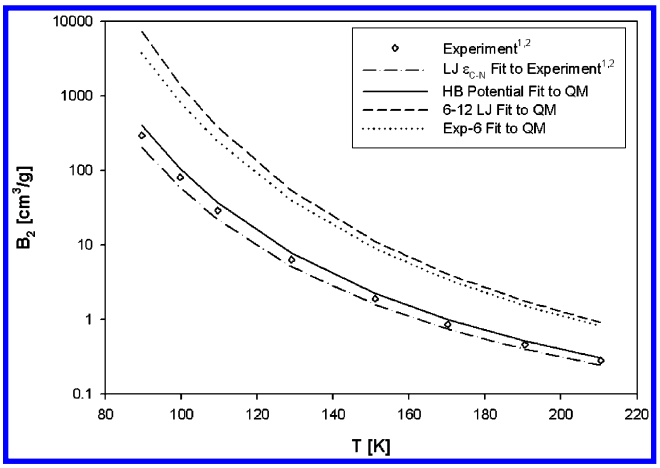

Figure 5. Second virial coefficients of nitrogen adsorption on graphite as a function of temperature calculated with the different potentials.

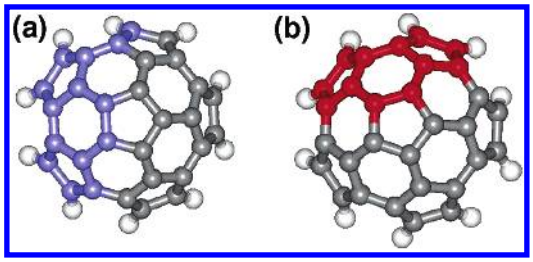

Figure 6. The cuts to the 30-carbon piece of C_{60}. (a) N_2−C_{168} calculations: 16-carbon segment in gray and 14-carbon segment in blue. (b) O_2−C_{168} calculations: 18-carbon segment in gray and 12-carbon segment in red.

Fourteen nitrogen−carbon interaction energies were calculated by using MP2−4:CC with the same SBS, MBS, and LBS as was used with benzene. The location of nitrogen was within the well region of the potential for all but two of the orientations. Two of the well points were near the crossing point of the potential, which has been shown previously to be important in the fitting of a potential to quantum mechanically calculated energies.[40] The final two positions result in repulsive nitrogen−C_{60} interactions. The nitrogen−carbon surface interactions ranged from −5.3 to 4.3 kJ/mol, and each required approximately 15.8 days of single-processor CPU time, for a total of 222 days for the 14 points studied.

The calculation of the interaction energies of oxygen with the C_{60} surface (and also for the C_{168} surface) proved to be more difficult than that for nitrogen. In its ground state, oxygen is an open-shell molecule with two singly occupied orbitals, while nitrogen is a close-shell molecule. The simplest method to calculate QM energies of an open-shell molecule is to use the unrestricted determinate (UHF, UMP2, etc.). However, this can result in so-called spin contamination (a calculated spin that differs from the true state),[41] and for the O_2−C_{60} system a poor initial guess for the orbital coefficients results in these singly occupied orbitals being placed on the carbon surface instead of the oxygen. The restricted open-shell (RO) determinant, which is an eigenfunction of the spin operator, is commonly used to alleviate the spin contamination problem at the cost of increased computational time.[41] However, the Gaussian 98 package[34] can only be used to calculate ROMP2 energies, but not the ROHF reference states for MP4(SDQ) or CCSD(T), which are needed to eliminate spin contamination in MP2−4:CC. Alternatively, by using a converged ROHF wave function as the initial guess in UMP4(SDQ) or UCCSD(T), negligible spin contamination and proper orbital placement is obtained in the final wavefuntions. Therefore, this approach was used for the UMP4(SDQ)/MBS and UCCSD(T)/SBS calculations in eq 3 (and their resulting MP2/MBS and MP4(SDQ)/SBS calculations) and ROMP2 was used for the MP2/LBS calculation in eq 3.

For C_{60} the 14−16 segment cut used for nitrogen resulted in large spin contamination and incorrect interaction energies in the oxygen calculation. A 12−18 cut (Figure 6b), which was found to be accurate and did not result in spin contamination, was used for the oxygen−carbon interaction energy calculations. Then only the 18-carbon segment was used to develop the O_2−C_{60} potential to reduce the computational time, which was about twice that for a similar calculation with nitrogen. Oxygen was placed near the 18-carbon fragment, shown in Figure 6b, to avoid any significant interactions with the 12-carbon segment.

A total of 10 oxygen−carbon interaction energies were calculated with the MP2−4:CC method, and ranged in value from −4.0 to 5.0 kJ/mol. Eight oxygen positions were located in the well of the potential: one point was near the potential crossing point and another was in the repulsive region. The MP2−4:CC interaction energies required a total of 290 CPU days for the 10 orientations of O_2 interacting with the 18-carbon segment.

Gas atom site−C_{60} potentials were then fit to these calculated interaction energies to compare with the gas−graphite interactions. However, since the carbon surface of C_{60} is curved, the planar and highly symmetric resonance structure present in graphite is absent in the C_{60} fullerene with its five-membered rings. This changes the underlying basis of the γ_A parameter (related to the polarizability of a carbon atom perpendicular to the graphite sheet and the dipole moment of the nitrogen or oxygen[39]) and the charge repulsion γ_R parameter in eq 7. For the C_{60} fullerene, θ in eq 7 is the angle between the vector along the gas molecule axis and the surface normal at each carbon atom, so that there is a different value of θ for each gas−carbon atom interaction (similarly for R_{iz} in eq 8), while in graphite the unique values θ and R_{iz} for a single diatom orientation result in an anisotropic contribution to the gas−graphite potential. Here, however, these contributions are different for the different orientations of each carbon atom in the C_{60} and C_{168} structures, and therefore should result in a less corrugated potential.

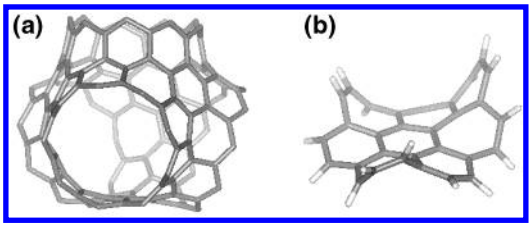

Figure 7. (a) C_{168} tetrahedral channel intersection and (b) 30 carbon piece used in QM calculations.

TABLE 3: Atom Site Potential Parameters of Nitrogen and Oxygen for Various Carbon Surfaces

guest	carbon surface	potential	AAD [kJ/mol]	ϵ/k	σ [Å]	γ_R	γ_A
N_2	graphite	Steele[4,5]		33.4	3.36		
	C_{60}	6-12 LJ	0.220	36.704	3.403		
		HB	0.235	34.376	3.428	−0.003	0.031
		HB, $e_{cq} = 0$	0.218	36.562	3.405	−0.004	0.001
	C_{168}	6-12 LJ	0.845	36.902	3.542		
O_2	graphite	Steele[4,5]		37.6	3.19		
	C_{60}	6-12 LJ	0.177	34.957	3.345		
		HB	0.290	34.964	3.345	−0.002	0.000
		HB, $e_{cq} = 0$	0.179	34.952	3.345	−0.001	0.000
	C_{168}	6-12 LJ	0.870	35.128	3.269		

The HB potential parameters shown in Table 3 (including the charge-quadrupole term and $e_{cq} = 0$) were obtained by fitting the interaction energies of nitrogen and separately of oxygen with the C_{60} fragment. For all the parameter fits shown, the values of ϵ/k and σ are nearly identical with those of the LJ 6-12 fit, and the values of the anisotropic parameters γ_R and γ_A obtained are so small that they can be neglected. For the nitrogen−C_{60} interaction, there is a slight change in the ϵ/k and σ values between the isotropic and anisotropic potential (including the charge-quadrupole term), but it is smaller than was the case for nitrogen and graphite. The smallest difference between the LJ 6-12 and HB potential parameters was found for $e_{cq} = 0$, but setting this term to zero in the nitrogen−graphite potential resulted in nearly identical parameter values as for the complete HB potential. Therefore, we conclude that the anisotropic HB potential reduces to the isotropic LJ 6-12 potential for the C_{60} surface due to the changing values of θ and R_{iz} in eqs 7 and 8 for each carbon atom in the surface.

C_{168} Schwarzite. The C_{168} schwarzite, which has a similar average radius of curvature[15] to that of the C_{60} fullerene, was the final carbon surface considered. The common repeating unit in C_{168} is a tetrahedral channel intersection containing 84 carbon atoms (a slightly larger section is shown in Figure 7a with 120 carbon atoms). A 30-carbon piece of C_{168} structure was again used to develop the intermolecular potentials (see Figure 7b). This carbon cluster, with hydrogens added along the cleaved bonds, is assumed to be large enough to represent the curvature of the carbon surface in this schwarzite, so that interaction energies calculated should represent the interaction for the same piece of a C_{168} schwarzite.

Similar to graphite and C_{60}, the 30-carbon piece in Figure 7b requires an additional cut to calculate interaction energies

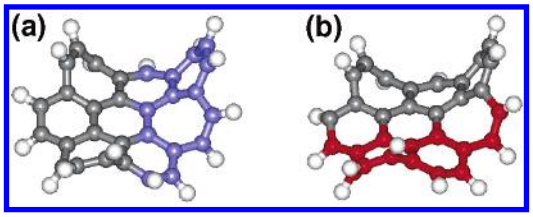

Figure 8. The cuts to the 30-carbon piece of C_{168}. (a) N_2-C_{168} calculations: 16-carbon segment in gray and 14-carbon segment in blue. (b) O_2-C_{168} calculations: 16-carbon segment in gray and 14-carbon segment in red.

at the MP2−4:CC level, and this is shown in Figure 8. Using an approach similar to that used for graphite and C_{60}, the 14−16 cut shown in Figure 8a was found to accurately represent the nitrogen−carbon interaction at several small basis sets.

Four favorable equilibrium positions and orientations of nitrogen and oxygen in C_{168} obtained from GCMC simulations with the Steele potential[42] were used to calculate the ab initio binding energies. The MP2−4:CC method was used with the same SBS, MBS, and LBS as described earlier. The two-step HM-IE method for this system required between 18 and 23 days of CPU time for each position (depending on the location of the gas molecule) even with the reduced convergence criteria for the CCSD(T) energy and wave function mentioned earlier.

A total of eight binding energies were calculated with one close to the crossing point of the potential and another being repulsive. The QM-calculated interaction energies varied from −9.9 to +10.3 kJ/mol, and an unweighted objective function was used in fitting. The result of the LJ 6-12 potential fit is shown in Table 3. Since for C_{60} the HB potential reduces to the LJ 6-12 potential, only this latter potential was fit for this similarly curved carbon surface.

For oxygen interacting with C_{168} an identical approach was unsuccessful for the 30-carbon surface cut used above, but an equally accurate 14−16 cut resulted in correct unrestricted energies (see Figure 8b). In some calculations, the cut piece at the greatest distance from the O_2 molecule resulted in incorrect spins on that carbon surface. Therefore, when oxygen was placed near a 16-carbon segment, only the interactions with that segment were computed. For this 16-carbon segment, each MP2−4:CC calculation requires about 20 CPU days with the same SBS, MBS, and LBS as was used for nitrogen. The six binding energies ranged from −7.5 to +0.24 kJ/mol and an unweighted objective function was used to obtain the LJ 6-12 potential parameters in Table 3.

Comparing the Interaction Potentials

Although the LJ 6−12 potential is known to result in a poor description of the gas−graphite potential surface, the widely used Steele potential has been parametrized to this functional form, which allows for a direct comparison with our QM-based gas−C_{60} and gas−C_{168} potentials.

As shown in Table 3, there are differences in the values of the gas−carbon potential parameters between graphite and the curved carbon surfaces. The values of the σ parameter in the LJ potential vary the most between the Steele potential and those obtained here for the curved surfaces, although there are also slight differences in the ϵ/k values. The well depth of the nitrogen−carbon potential is larger and the oxygen−carbon well depth is smaller than in the Steele potential, while the values of σ are consistently larger than in the Steele potential.

The difference in surface curvature between graphite and a curved carbon sheet is the likely source of the differences in potentials for a gas interacting with these carbons. In graphite the π electron clouds are on "planar" rings over the six-membered rings; however, in C_{60} and C_{168} the surfaces have a positive curvature with respect to the gas molecule. Therefore, an adsorbing molecule is more likely to be closer to a graphite surface than the curved carbon surface which results in a closer contact with neighboring carbon rings and a more diffuse electron cloud. This changes the crossing point of the potential, which may lead to larger σ values in the gas−C_{60} and gas−C_{168} potentials than in the gas−graphite potentials. Also small changes in the carbon orbital/electron clouds between the carbon schwarzite or buckyball and graphite may be the reason for the slight differences in the fitted values of ϵ/k.

TABLE 4: Interaction Energies in (kJ/mol) for the N_2-C_{168} 30-Carbon Piece at Various Positions

orientation no.	QM	LJ fit to QM C_{168}	LJ fit to QM C_{60}	LJ fit to QM graphite	Steele potential
1	−9.940	−9.883	−9.013	−9.847	−7.892
2	−7.534	−6.627	−5.379	−5.438	−4.580
3	−7.398	−7.613	−6.786	−7.311	−5.911
4	−4.720	−6.147	−7.367	−9.212	−6.795
5	−3.169	−2.542	−2.013	−1.997	−1.703
6	−0.178	−0.974	−0.765	−0.754	−0.645
7	0.473	2.389	−2.444	−5.724	−3.044
8	10.324	9.486	1.478	−3.125	−0.110

These variations in the atom-site parameters of the LJ potential can result in large energy differences for gases interacting with the different carbon surfaces. An example of this is shown in Table 4 for diatomic nitrogen and the 30-carbon piece of C_{168}. For orientations 1 and 3, QM-based N_2−graphite LJ potential accurately represents the binding energies of nitrogen on C_{168}, because these are at a distance where the potentials cross, as will be discussed later. However, the other orientations are poorly described by the QM-based N_2−graphite LJ potential. The interaction energies for the crossing point and repulsive wall, orientations 7 and 8, are not correctly described by the Steele and graphite-based QM LJ potentials, as the value of the LJ σ in these potentials is smaller than that fitted directly to the N_2-C_{168} QM interactions (compare Tables 2 and 4).

Differences also exist between the interaction energy predictions with the N_2-C_{168} and N_2-C_{60} potentials. The largest difference occurs near the crossing point of the potential, where the C_{60}-based potential results in more attractive interaction energies. The 0.139 Å variation in the σ parameter is the cause of the difference in the N_2-C_{60} and N_2-C_{168} potentials, and since C_{168} and C_{60} have similar carbon surface curvatures, this variation in the potential parameters is probably due to the difference in ring structures, i.e., seven- and five-membered rings, respectively. However, for oxygen−carbon interactions this ring structure change results in a value of σ that is slightly larger with C_{60} than with C_{168}.

Even though the C−N well depth and collision diameter of the HM-IE based LJ potential are only slightly larger than the values reported by Steele, this results in a significant effect on the N_2-C_{168} potential in the C_{168} channel intersection (Figure 7a); see Figure 9a. The N_2-C_{168} channel intersection potential depth is significantly lower than that computed with the Steele potential (r < 2.9 Å, where r is measured from the center of the channel), and the repulsive wall is steeper (r > 3.5 Å). The QM-based N_2−graphite and N_2-C_{168} potentials cross at about 2.2 Å from the center of the channel interaction, which results in similar energies for orientations 1 and 3 in Table 4. As shown in Figure 9a, the O_2-C_{168} channel intersection binding energy of the HM-IE based potential is similar to that of the Steele potential, but is slightly more attractive for distances less than 2.9 Å.

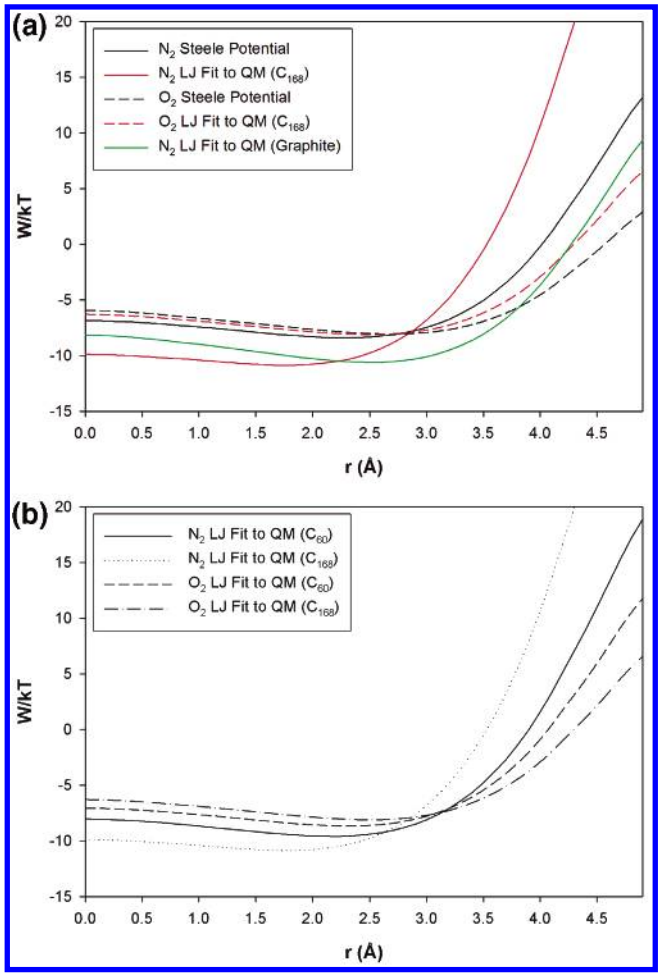

Figure 9. Nitrogen and oxygen C_{168} channel intersection binding energies at 298 K, where *r* is the distance from the center of the channel intersection

The graphite-based Steele potential results in similar binding energies for N_2 and O_2 up to 2.5 Å from the center of the channel intersection. However, as seen in Figure 9a, the binding energy of nitrogen at the center of the channel intersection is 74% more attractive than for oxygen computed with use of the LJ potential that has been fit to QM interaction energies with C_{168}. The binding energy difference between nitrogen and oxygen is reduced for the gas−C_{60} potential (see Figure 9b), but the nitrogen interaction is more attractive in the C_{168} channel interaction than oxygen by 14%. Since the major difference between C_{60} and C_{168} is their ring structure, presumably it is the replacement of five-membered rings with seven-membered rings in C_{168} that results in the increased adsorption energies of nitrogen over oxygen.

The two QM-based potentials and the Steele O−C potential result in similar predictions for the oxygen−carbon interaction energies in the C_{168} channel intersection. Consequently, it appears that the carbon surface curvature and ring structure have only a minor effect on the oxygen−carbon interaction, while there is a strong effect on the nitrogen−carbon interaction. This may be the result of oxygen being an open-shell molecule and nitrogen being a closed-shell molecule.

Conclusions

We have found that MP2 calculations overestimate the binding energies of nitrogen and oxygen with carbon surfaces, and that higher levels of theory are required. A two-step HM-IE method was used to approximate CCSD(T)/LBS results with reasonable levels of accuracy and computational efficiency, and this was proven for the interactions of nitrogen and oxygen with benzene. This method was then used to develop a N_2−graphite potential. The HB potential, which accounts for the corrugation of the planar graphite surface, with parameters fitted to the results of the quantum mechanics calculations was found to lead to accurate predictions of the measured values of the second virial coefficient for adsorption; this form of the potential had been found previously to improve predictions of inelastic neutron scattering. Thus, this work supports the conclusion that detailed potentials are required for nitrogen, and most likely oxygen, interacting with graphite. However, the HB potential was found to be equivalent to the isotropic LJ 6-12 potential for the curved carbon surface of C_{60}.

Quantum mechanically based LJ 6-12 potentials for nitrogen and oxygen interacting with carbon in the C_{60} and C_{168} structures resulted in different gas−carbon interactions (and potential parameters) compared to interactions with planar graphite. Using these potentials, we found that carbon surface curvature and ring structure are important for the predicted nitrogen−C_{168} channel intersection interaction energies. However, for the carbon surfaces studied here, the oxygen−carbon potentials resulted in only slight changes in the energies at the C_{168} channel intersection. Overall, there is a significant difference between the N_2 and O_2 binding energies in the C_{60} and C_{168} structures with use of our QM-based potential compared to those obtained with the Steele potential. This will result in pronounced differences between the predicted adsorption isotherms, and possibly the diffusion coefficients, of these two gases in C_{168}, which may explain the differences in oxygen and nitrogen permeabilities measured by Shiflett and Foley.[2,3]

Acknowledgment. We would like to acknowledge the financial support of this research from contract CTS-0083709 and EEC-0085461 from the U.S. National Science Foundation. We especially wish to acknowledge the many contributions of Professor Douglas Doren of the Department of Chemistry and Biochemistry of the University of Delaware for his advice and assistance throughout this work, and his detailed comments on the initial version of this paper that resulted in changes and improvements. The work we presented here was carried out mainly at the University of Delaware.

References and Notes

(1) Baker, R. W. *Ind. Eng. Chem. Res.* **2002**, *41*, 1393.
(2) Shiflett, M. B.; Foley, H. C. *J. Membr. Sci.* **2000**, *179*, 275.
(3) Shiflett, M. B.; Foley, H. C. *Science* **1999**, *285*, 1902.
(4) Bojan, M. J.; Steele, W. A. *Langmuir* **1987**, *3*, 1123.
(5) Bojan, M. J.; Steele, W. A. *Langmuir* **1987**, *3*, 116.
(6) Ohba, T.; Murata, K.; Kaneko, K.; Steele, W. A.; Kokai, F.; Takahashi, K.; Kasuya, D.; Yudasaka, M.; Iijima, S. *Nano Lett.* **2001**, *1*, 371.
(7) Seo, Y. G.; Kum, G. H.; Seaton, N. A. *J. Membr. Sci.* **2002**, *195*, 65.
(8) Murata, K.; Kaneko, K.; Steele, W. A.; Kokai, F.; Takahashi, K.; Kasuya, D.; Hirahara, K.; Yudasaka, M.; Iijima, S. *J. Phys. Chem. B* **2001**, *105*, 10210.
(9) Kostov, M. K.; Cheng, H.; Cooper, A. C.; Pez, G. P. *Phys. Rev. Lett.* **2002**, *89*, article no. 146105.
(10) Klauda, J. B.; Sandler, S. I. *J. Phys. Chem. B* **2002**, *106*, 5722.
(11) Schwarz, H. A. *Gesammelte Mathematische Abhandlungen*; Springer: Berlin, Germany, 1890.
(12) King, R. B. *Jo. Phys. Chem.* **1996**, *100*, 15096.
(13) Huang, M. Z.; Ching, W. Y.; Lenosky, T. *Phys. Rev. B* **1993**, *47*, 1593.
(14) Okeeffe, M.; Adams, G. B.; Sankey, O. F. *Phys. Rev. Lett.* **1992**, *68*, 2325.
(15) Vanderbilt, D.; Tersoff, J. *Phys. Rev. Lett.* **1992**, *68*, 511.
(16) Lenosky, T.; Gonze, X.; Teter, M.; Elser, V. *Nature* **1992**, *355*, 333.

(17) Townsend, S. J.; Lenosky, T. J.; Muller, D. A.; Nichols, C. S.; Elser, V. *Phys. Rev. Lett.* **1992**, *69*, 921.

(18) David, W. I. F.; Ibberson, R. M.; Matthewman, J. C.; Prassides, K.; Dennis, T. J. S.; Hare, J. P.; Kroto, H. W.; Taylor, R.; Walton, D. R. M. *Nature* **1991**, *353*, 147.

(19) Kroto, H. W.; Heath, J. R.; Obrien, S. C.; Curl, R. F.; Smalley, R. E. *Nature* **1985**, *318*, 162.

(20) Wesolowski, T. A.; Parisel, O.; Ellinger, Y.; Weber, J. *J. Phys. Chem. A* **1997**, *101*, 7818.

(21) Lushington, G. H.; Chabalowski, C. F. *THEOCHEM* **2001**, *544*, 221.

(22) Lee, S.; Romascan, J.; Felker, P. M.; Pedersen, T. B.; Fernandez, B.; Koch, H. *J. Chem. Phys.* **2003**, *118*, 1230.

(23) Klauda, J. B.; Garrison, S. L.; Jiang, J.; Arora, G.; Sandler, S. I. *J. Phys. Chem. A* **2004**, *108*, 107.

(24) Lide, D. R. *CRC Handbook*, 81 ed.; CRC Press: Boca Raton, FL, 2000.

(25) Curtiss, L. A.; Redfern, P. C.; Raghavachari, K.; Rassolov, V.; Pople, J. A. *J. Chem. Phys.* **1999**, *110*, 4703.

(26) Curtiss, L. A.; Raghavachari, K.; Redfern, P. C.; Rassolov, V.; Pople, J. A. *J. Chem. Phys.* **1998**, *109*, 7764.

(27) Dunning, T. H.; Peterson, K. A. *J. Chem. Phys.* **2000**, *113*, 7799.

(28) Huh, S. B.; Lee, J. S. *J. Phys. Chem. A* **2002**, *106*, 10606.

(29) Tsuzuki, S.; Honda, K.; Uchimaru, T.; Mikami, M.; Tanabe, K. *J. Am. Chem. Soc.* **2002**, *124*, 104.

(30) Tsuzuki, S.; Uchimaru, T.; Mikami, M.; Tanabe, K. *J. Phys. Chem. A* **2002**, *106*, 3867.

(31) Tsuzuki, S.; Honda, K.; Uchimaru, T.; Mikami, M.; Tanabe, K. *J. Phys. Chem. A* **1999**, *103*, 8265.

(32) Koch, H.; Fernandez, B.; Christiansen, O. *J. Chem. Phys.* **1998**, *108*, 2784.

(33) Klopper, W.; Luthi, H. P. *Mol. Phys.* **1999**, *96*, 559.

(34) Frisch, M. J.; Trucks, G. W.; Schlegel, H. B.; Scuseria, G. E.; Robb, M. A.; Cheeseman, J. R.; Zakrzewski, V. G.; Montgomery, J. A.; Stratmann, R. E.; Burant, J. C.; Dapprich, S.; Millam, J. M.; Daniels, A. D.; Kudin, K. N.; Strain, M. C.; Farkas, O.; Tomasi, J.; Barone, V.; Cossi, M.; Cammi, R.; Mennucci, B.; Pomelli, C.; Adamo, C.; Clifford, S.; Ochterski, J.; Petersson, G. A.; Ayala, P. Y.; Cui, Q.; Morokuma, K.; Malick, D. K.; Rabuck, A. D.; Raghavachari, K.; Foresman, J. B.; Cioslowski, J.; Ortiz, J. V.; Stefanov, B. B.; Liu, G.; Liashenko, A.; Piskorz, P.; Komaromi, I.; Gomperts, R.; Martin, R. L.; Fox, D. J.; Keith, T.; Al-Laham, M. A.; Peng, C. Y.; Nanayakkara, A.; Gonzalez, C.; Challacombe, M.; Gill, P. M. W.; Johnson, B. G.; Chen, W.; Wong, M. W.; Andres, J. L.; Head-Gordon, M.; Replogle, E. S.; Pople, J. A. *Gaussian 98*, Revision A.9; Gaussian, Inc: Pittsburgh, PA, 1998.

(35) Boys, S. F.; Bernardi, F. *Mol. Phys.* **1970**, *19*, 553.

(36) Feller, D.; Jordan, K. D. *J. Phys. Chem. A* **2000**, *104*, 9971.

(37) Hansen, F. Y.; Bruch, L. W. *Phys. Rev. B* **1995**, *51*, 2515.

(38) Hansen, F. Y.; Bruch, L. W.; Roosevelt, S. E. *Phys. Rev. B* **1992**, *45*, 11238.

(39) Carlos, W. E.; Cole, M. W. *Surf. Sci.* **1980**, *91*, 339.

(40) Garrison, S. L.; Sandler, S. I. *J. Chem. Phys.* **2002**, *117*, 10571.

(41) Szabo, A.; Ostlund, N. S. *Modern Quantum Chemistry*: *Introduction to Advanced Electronic Structure Theory*; Dover Publication, Inc.: Mineola, 1996.

(42) Jiang, J.; Klauda, J. B.; Sandler, S. I. *Langmuir* **2003**, *19*, 3512.